J Nanopart Res (2023) 25:98
https://doi.org/10.1007/s11051-023-05751-0

RESEARCH PAPER

In situ growth of Ag nanoparticles on pristine graphene and their applications in conductive ink

Lei Zhu · Qin-Qin Xu · Jin Guo · Shuo-Lei Niu · Bao-Ning Lu · Jian-Zhong Yin

Received: 16 January 2023 / Accepted: 20 April 2023 / Published online: 3 May 2023

Abstract Graphene decorated with Ag nanoparticles can cross the defect and bridge the adjacent graphene sheets to enhance its conductivity, making the composite more suitable for conductive ink preparation rather than pure graphene. In this study, a facile one-pot method to prepare Ag NPs@graphene nanocomposite is proposed. Graphite is exfoliated by low-speed mechanical agitation and low-power ultrasonic to obtain pristine graphene, which has fewer structural defects and intrinsic defects than RGO. Then, Ag nanoparticles are in situ loaded on graphene with $AgNO_3$ as the precursor, PVP as the dispersant, and glucose as the reducing agent, solving the negative effect of grain boundaries and overlap defects. Uniformly dispersed Ag nanoparticles are obtained anchored on or between the multi-layer graphene sheets. The average size of Ag nanoparticles is 56 nm. Finally, the prepared Ag NPs@graphene nanocomposite is used as conductive filler to prepare water-based conductive ink. At the optimal sintering temperature and time (150 °C for 20 min), the square resistance of the conductive patterns printed by screen printing is 21.6 mΩ sq^{-1}, indicating that the conductive ink has great potential applications in printed electronics.

L. Zhu · Q.-Q. Xu (✉) · J. Guo · S.-L. Niu · B.-N. Lu · J.-Z. Yin
State Key Laboratory of Fine Chemicals, School of Chemical Engineering, Dalian University of Technology, Dalian, China
e-mail: qinqinxu@dlut.edu.cn

Keywords Graphene · Ag NPs@graphene nanocomposite · One-pot method · Conductive ink · Printing electronics

Introduction

As a new technology, printed electronic technology has developed rapidly in recent years, which is an important innovation in the field of microelectronics. It is widely used in sensors, paper batteries, film switches, solar cells, radio frequency identification (RFID) smart tags, and other fields [1–6]. The core of printed electronics is to transfer the functional conductive ink to the substrate by printing, so that the printed patterns have conductivity to realize the production of electronic components [7, 8]. The key technology of printed electronics is the preparation of conductive ink, which contains functional conductive materials, so it can realize conductive function [9–11].

According to the different types of conductive fillers, conductive ink can be divided into inorganic conductive ink, organic conductive ink, and composite conductive ink. The conductive fillers of inorganic conductive inks are mainly Au, Ag, Cu, Ni, and other metal powders or metal nano-powders, as well as carbon black, graphite, and other non-metallic powders or particles. Muhammad Rizwan et al. [12] reported successful fabrication of RFID tag antennas by inkjet printing of copper nanoparticle ink on a Kapton

substrate and by thermal printing of copper material on a polyester-based substrate material (referred to as THERML film). A peak read range of 7–10 m for the thermal-printed tags on THERML film was obtained due to their excellent conductivity. The conductive fillers of organic conductive ink are conductive polymers with conjugated structure such as polyaniline; they are usually lighter, more flexible, and less expensive, compared to inorganic conductors. However, conductive organics usually exhibit low carrier mobility and inferior stability, compared with inorganic materials such as silicon or copper. Das et al. [13] obtained poly(3,4-ethylenedioxythiophene) (PEDOT) by oxidative polymerization of monomer and anhydrous ferric chloride in acetonitrile. After washing and ultrasonic treatment in water, a conductive ink based on PEDOT aqueous dispersion was obtained. It is printed on a glass substrate by air-brush technique to form a thin conductive film with a sheet resistance of 1~20 kΩ/sq. However, there is still a big gap of the conductivity between this ink and that of the metal filler ink. Composite conductive ink is prepared by compounding two or more different kinds of conductive fillers. Combined with the properties of different kinds of conductive fillers, different kinds of conductive materials can complement each other, so the performance of conductive ink can be greatly improved. Composite conductive ink is suitable for integrated circuits, electronic film switches, flexible electronic products, and other fields because of its high conductivity and excellent mechanical properties. It is a research hotspot in the field of conductive ink. Xu et al. [14] used N, N-dimethylformamide as a reducing agent to reduce Ag nanoparticles from $AgNO_3$ solution and uniformly adhere to the graphene sheet. Then, the composite was used as a conductive filler, and a certain proportion of ethanol, ethylene glycol, and glycerol mixture were used as a matrix to prepare a pen for direct writing. When the printed conductive track was solidified at 100 °C for 60 min, a typical resistivity value measured was 1.9×10^{-7} Ω•m.

As a one-atom-thick planer sheet of sp^2-hybridized carbon atoms, graphene is an ideal carbon material for preparation of conductive ink because of its superior carrier mobility (15,000 $cm^2 \bullet V^{-1} \cdot s^{-1}$), high specific surface area (2630 $m^2 \bullet g^{-1}$) and mechanical strength (1.0 TPa) [15–17]. Besides the eco-friendliness, using graphene as conductive filler of conductive ink has many other advantages, such as light weight, low processing temperature, and especially low, cost compared to metallic materials. However, due to the grain boundaries and overlap defects between graphene flakes, the specific conductivity of the conductive ink made by pure graphene is two or three orders of magnitude smaller than that of pure metal materials. With outstanding conductivity, heat conduction, and flexibility, Ag nanoparticles were usually considered as good potential candidates for conductive fillers. Nevertheless, Ag nanoparticles or nanowires exhibit large specific surface areas, and result in the exacerbation of oxidation process [18] due to a large area explosion to the surrounding. When Ag nanomaterials and graphene are combined, the former can cross the defect and bridge the adjacent graphene sheets, solving the negative effect of grain boundaries and overlap defects. In the meanwhile, graphene sheets are tiled between Ag conductive network and patched it up, thereby increasing the carrier concentration. With excellent gas blocking performances, graphene can also form a passive layer to prevent oxidation [19].

Most of the reported methods for the preparation of Ag NPs@graphene nanocomposite are based on the attachment of Ag nanoparticles on the graphene oxide (GO) and reduced GO (rGO) [20–26], and rGO is prepared by laser-induced, chemical reduction, or thermal reduction method from GO [27, 28]. However, rGO contains a large number of oxygen-containing functional groups, resulting in structural defects and inherent defects, thus its conductivity is much lower than that of the pristine graphene.

Herein, we proposed a simple and mild in situ growth of Ag nanoparticles on pristine graphene to prepare Ag NPs@graphene nanocomposite and then prepared the conductive inks. Natural graphite was chosen as initial materials and after pristine graphene was obtained by exfoliation in N-methylprolinodone (NMP) by mechanical agitation, the silver ammonia solution was directly added into the graphene-NMP solution after filtration and removal of the unexfoliated graphite. Then polyvinylpyrrolidone (PVP) was added as a dispersant for Ag nanoparticles, and glucose was added as a reducing agent to reduce Ag nanoparticles. PVP can also act as the dispersant of graphene. Ag nanoparticles were anchored on the surface of graphene or intercalated between the graphene sheets, avoiding the aggregation of the exfoliated graphene. Scanning electron microscope (SEM), UV-vis spectrometry,

and XRD (X-ray diffraction) were used to characterize the morphology and the size of the composite. Raman characterization was used to prove that Ag nanoparticles were loaded on the graphene sheets. The influence of the mass ratio of graphite powder to $AgNO_3$, the molar ratio of PVP to $AgNO_3$, the concentration of glucose, and the reaction temperature on Ag nanoparticle dispersion and size were investigated. Then, the prepared Ag NPs@graphene nanocomposite was used as conducting filler to prepare conductive ink.

Materials and methods

Materials

Natural graphite flakes (1000 mesh) with carbon content of 99.9% were obtained from QingDao Risheng Graphite Ltd. Prior to using them, they were dried overnight in the oven at 120 °C. $AgNO_3$, glucose, and polyvinyl pyrrolidone (PVP) of analytical grade were purchased from Sinopharm. Deionized water (H_2O) was obtained by reverse osmosis followed by ion exchange and filtration. Ethanol (EtOH, analytically pure, > 99.7%), N-methyl pyrrolidone (NMP), and aqueous ammonia (AR, 25%) were commercially provided by Tianjin Kemiou Chemical Reagent Co., Ltd. Watercraft acrylic resin was supplied by Shanghai Wenhua Chemical Co., Ltd. Leveling agent, ph regulator, defoaming agent, and thickening agent were supplied by Guangzhou Runhong Chemical Co., Ltd. All the materials were used without further purification.

Brief introduction of leveling agent, ph regulator, defoaming agent, and thickening agent:

The leveling agent is an organic modified polydimethylsiloxane solution, which is a highly active water-soluble additive. It can promote the ink to form a flat, smooth, and uniform coating film during the drying process.

The pH regulator is 95% aqueous solution of 2-amino-2-methyl-1-propanol. It is used to change the pH of ink.

The defoaming agent is polyether-modified polydimethylsiloxane. It is an additive for eliminating foam.

The thickening agent is an acrylate polymer. It is used to increase the viscosity of ink.

Preparation of Ag NPs@graphene nanocomposite and water-based conductive ink

As shown in Fig. 1 a, 0.5 g of natural graphite flake and 50 mL of NMP were initially put in a stainless steel reactor. The reactor was sealed, and the materials were agitated by a three-blade type propeller with a speed of 3000 rpm at the room temperature for 3 h. Then, the mixture of NMP and the semi-exfoliated graphite was subject to bath sonication (KQ2200DB, 100 W, and 40 kHz) for 100 W for 1 h. The dispersion was subject to natural sedimentation for 20 min, and 60% of the middle fraction was taken for further use. A certain amount of $AgNO_3$ (0.25–2g) was weighed and put into a beaker, and a certain amount of water was added to prepare a certain concentration of $AgNO_3$ solution. Then, ammonia water was added drop by drop, and the solution was stirred while dropping until the initial precipitation was dissolved. The preparation of silver ammonia solution was completed. Then, the graphene dispersion and ammoniacal silver solution were added into the reactor, and then a certain amount of PVP was added too (The molar ratio of PVP to $AgNO_3$ was 1~3). When the temperature reached 30~70 °C, the glucose solution (0.3~2 mol/L) was added dropwise in the reactor. After 1-h reaction, the mixture was centrifuged (10,000 r/min, 10 min) and washed for several times, and then it was air-dried for 4 h at 50 °C. Finally, Ag NPs@graphene nanocomposite was obtained. For the Ag NPs@graphene nanocomposite, the dispersed graphene sheets acted as the bridge to connect Ag nanoparticles, so they form a conductive network together (Fig. 1b). Watercraft acrylic resin (12 wt%), ethylene glycol (3 wt%), flow agent (0.7 wt%), ph regulator (0.3 wt%), Ag NPs@graphene nanocomposite (50 wt%), defoaming agent (0.5 wt%), thickening agent (1.5 wt%), and deionized water (32 wt%) were mixed and stirred to prepare conductive ink. The preparation process is shown in Fig. 2 a, and the prepared conductive ink photo is shown in Fig. 2 b.

Printing conductive patterns

Conductive patterns were obtained by screen printing the as-prepared conductive ink on the PI substrates using a screen mesh (200 mesh). The printing process was performed with a printing speed of ~40 mm s^{-1}, a printing force of ~30 N,

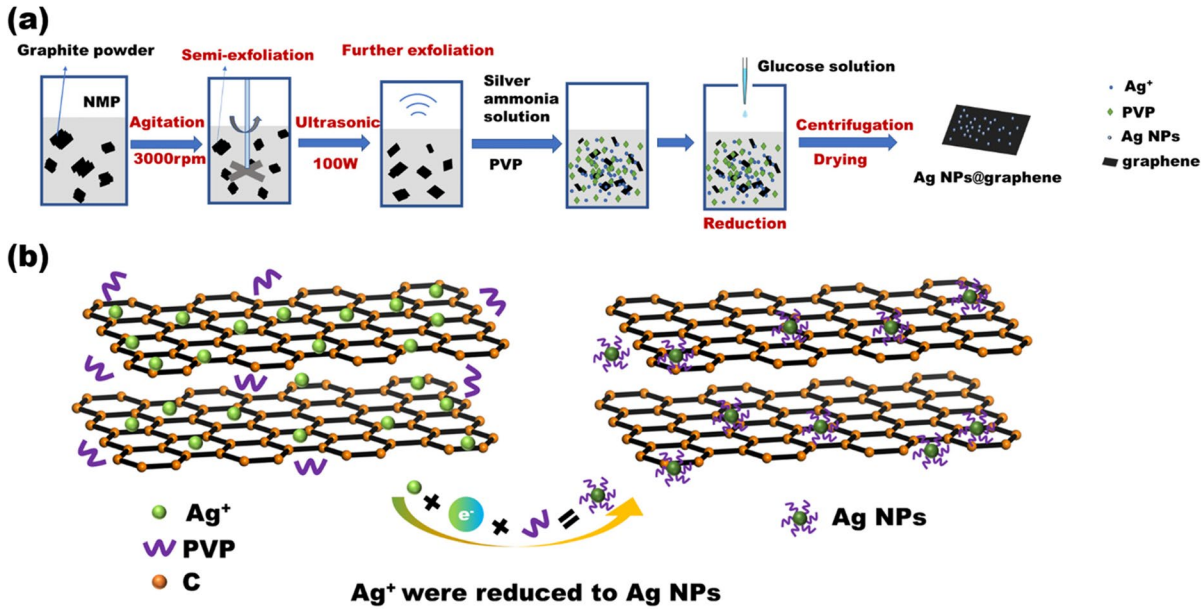

Fig. 1 Schematic of preparation of Ag NPs@graphene nanocomposite. **a** Exfoliation of graphite and formation of Ag nanoparticles. **b** Demonstration of Ag nanoparticles anchored on and interaction in the graphene sheets

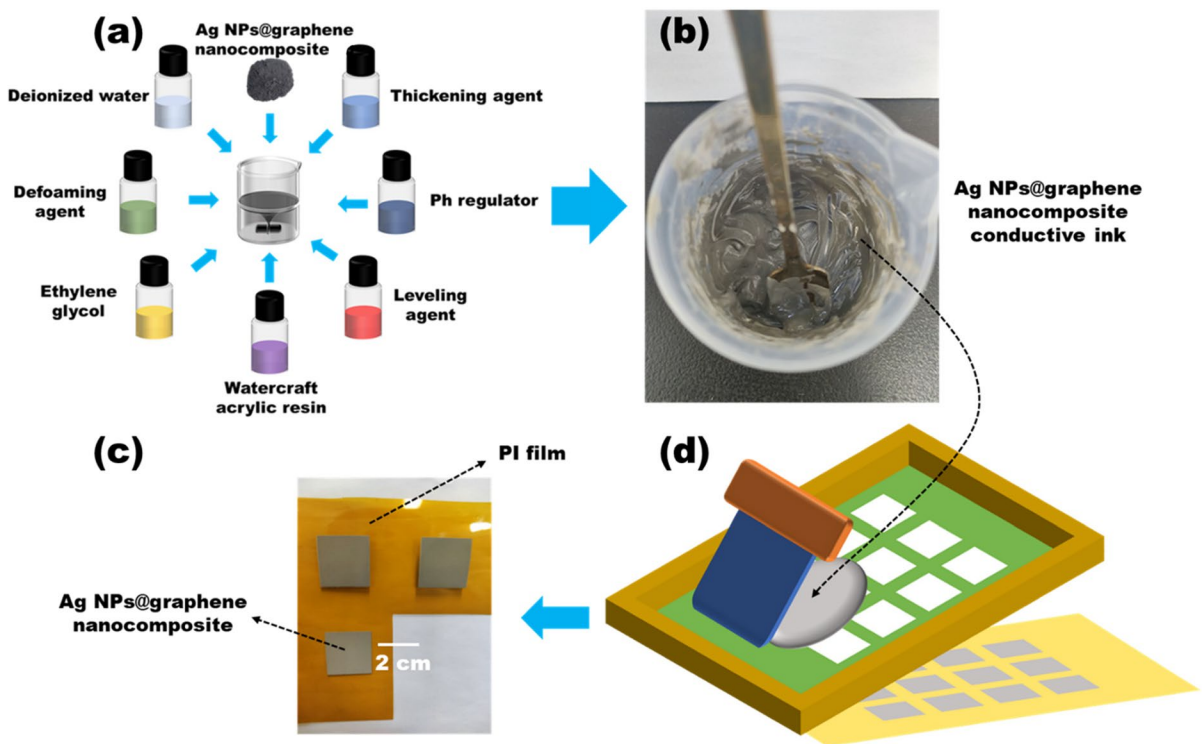

Fig. 2 **a** Preparation schematic of Ag NPs@graphene nanocomposite conductive Ink. **b** Photographs of Ag NPs@graphene nanocomposite conductive ink prepared. **c** Patterns were printed on PI film by screen printing. **d** The schematic of screen printing

and a printing angle of ~45°, as shown in Fig. 2 d. Finally, the printed patterns were annealed at 80~250 °C for 5 to 30 min to make the printed patterns form conductive networks. The printed patterns are shown in Fig. 2 c.

Characteristics and electrical properties of Ag NPs@graphene nanocomposite and conductive ink

The size and morphology of the Ag NPs@graphene nanocomposite were characterized by scanning electron microscopy (SEM) on a SU 5000 instrument at 15 kV. Ag nanoparticles were monitored by Lambda 750S UV-vis spectrometry in the range of 300~800 nm. An X-Pert Pro X-ray diffractometer was used to obtain the composition of the Ag NPs@graphene nanocomposite. XRD patterns were collected with a D/Max-βb diffractometer equipped with a Cu Kα radiation source (λ = 0.15432 nm) and operated at 40 kV and 30 mA. A continuous mode was used for collecting data from 10° to 90° of 2θ at a scanning speed of 5°/min. The Raman spectroscopy measurements were carried out using a DXR Microscope Raman spectrometer with 532 nm excitation. The square resistance of the ink-printed films and composite were measured using a HPS 2662 four-point probe analyzer. The square resistance of the composite was measured after the powder was pressed into tablets (taking 20 mg powder and then using YP-24 T powder tabletting machine produced by Tianjin Jinfulun Technology Co., Ltd. to tablet under 20 Mpa for 1 min). The thickness of ink-printed films and composites after tableting was measured using a micrometer.

Results and discussions

As shown in Fig. 3 a, the XRD pattern of the prepared Ag NPs@graphene nanocomposite was shown. By comparing with the PDF card in Jade software, it could be known that the position and intensity of the five diffraction peaks (111), (200), (220), (311), and (222) of the synthesized Ag nanoparticles were consistent with the diffraction peaks of silver (JCPDS No.04-0783)[29]. The characteristic diffraction peaks of graphene may be clearly seen, and no other impurity diffraction peaks were generated, which could be concluded that the Ag NPs@graphene nanocomposite was successfully prepared [30, 31].

Raman spectroscopy of fully dried graphene and Ag NPs@graphene nanocomposite at 50 °C is shown in Fig. 3 b and c. In the Raman spectrum of graphene, the G peak was caused by the E_{2g} vibration of the ordered sp^2 carbon atom, representing the degree of graphitization, while the D peak was caused by the sp^3 carbon atom and edge defects caused by the oxygen-containing functional group, representing the degree of oxidation [32]. It was reported [33] that the experimental intensity ratio I_D/I_G can be used to evaluate the defect nature of graphene. The D peak and G peak of graphene obtained by mechanical stripping and ultrasonic cavitation appeared at 1342.4 and 1567.9 cm^{-1} (Fig. 3c, I_D =59.4, I_G =430.0, and $R = I_D/I_G = 0.14$), far lower than the R-value in the literature (0.9–1.4) [32], indicating that the graphene prepared by our method had few defects, compared with rGO. The D and G peaks of the Ag NPs@graphene nanocomposite appeared at 1352.0 and 1578.6 cm^{-1} (Fig. 3b, I_D = 8539.2, I_G = 11874.6, and $R = I_D/I_G = 0.72$). It could

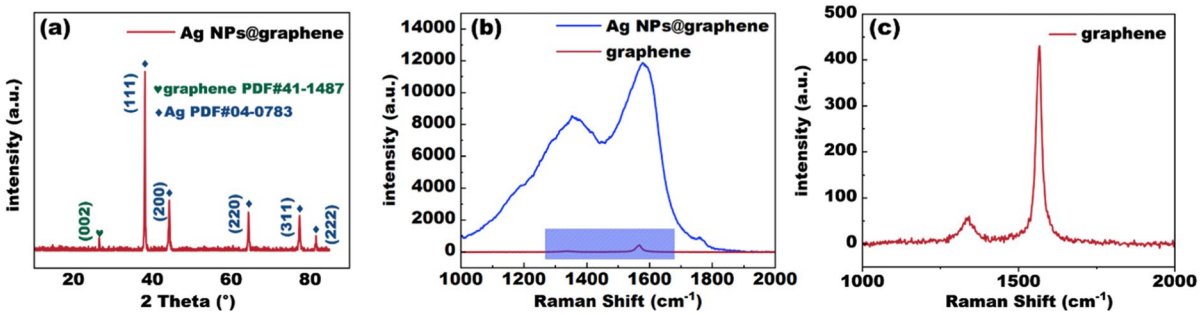

Fig. 3 **a** XRD pattern of the Ag NPs@graphene nanocomposite. **b** The Raman spectra of Ag NPs@graphene nanocomposite. **c** The Raman spectra of graphene (enlargement of the shaded portion of (**b**))

be seen from Fig. 3 b that the Raman signal intensity of the Ag NP-loaded graphene is much higher than that of the original graphene (Fig. 3c), indicating that Ag NPs were adsorbed on the graphene and enhanced the strength of the graphene.

Effect of different reaction conditions on properties of Ag NPs@graphene nanocomposite

Molar ratio of PVP to $AgNO_3$

The structure of PVP-contained hydrophilic groups (lactam groups) and hydrophobic groups (methylene groups), so it had good surface activity and could be used as a dispersant to prepare Ag nanoparticles. Due to the intramolecular and intermolecular forces between PVP and Ag^+, changing the molar ratio of PVP to $AgNO_3$ would affect the ion concentration in the solution, which would affect the thickness of PVP bounding to the silver seed and the position of PVP bounding to the seed, thus affecting the growth resistance of Ag nanoparticles in different directions [34–37].

To explore the effect of the amount of PVP on the microstructure of the prepared Ag NPs@graphene nanocomposite and the size of Ag nanoparticles, a set of comparative experiments of Ag NPs@graphene nanocomposite prepared with various molar ratios of PVP to $AgNO_3$ were characterized by SEM (Fig. 4a–d). In this set of experiments, the molar ratios of PVP to $AgNO_3$ were set to 1:1, 1.5:1, 2:1, 2.5:1, and 3:1, respectively. The other conditions were fixed as the mass ratio of $AgNO_3$ to graphite was 2:1; the concentration of glucose solution was 0.3 mol/L, and the reaction temperature was 60 °C.

When the molar ratio of PVP to $AgNO_3$ was 1:1 (Fig. 4a), the average size of the prepared Ag nanoparticles was 202 nm. This large size of the particles was attributed to the minor suppressed effect of PVP on the growth of Ag nanoparticles. When the mass ratio of PVP to $AgNO_3$ was 1.5:1 (Fig. 4b), the Ag nanoparticles and graphene were sufficiently dispersed, and the average size of Ag nanoparticles was 56 nm. When the molar ratio of PVP to $AgNO_3$ continuously increased to 2.5:1, the size of Ag nanoparticles gradually increased (239 nm). When the molar ratio of PVP to $AgNO_3$ increased to 3:1 (Fig. 4d), irregular shapes such as triangles and rods appeared, and the average particle size of Ag nanoparticles continued to increase to 345 nm. It showed that PVP inhibited the growth of some crystal planes resulting in uncontrollable shape [34–37].

According to Mie's theory [38], the position and shape of the absorption peak caused by surface plasmon resonance depend largely on the properties of metal nanoparticles, such as particle size, shape, and aggregation state. The effects of different molar ratios of PVP to $AgNO_3$ on the UV-vis absorption spectra of Ag NPs@graphene nanocomposite were demonstrated, as shown in Fig. 4 e. When the molar ratio of PVP to $AgNO_3$ was 1:1, the position of the absorption peak was near 500 nm, and the peak intensity in the long wavelength region was higher. When the molar ratio of PVP to $AgNO_3$ increased to 1.5:1, the position of the absorption peak moved to 428 nm approximately; the peak shape became symmetrical

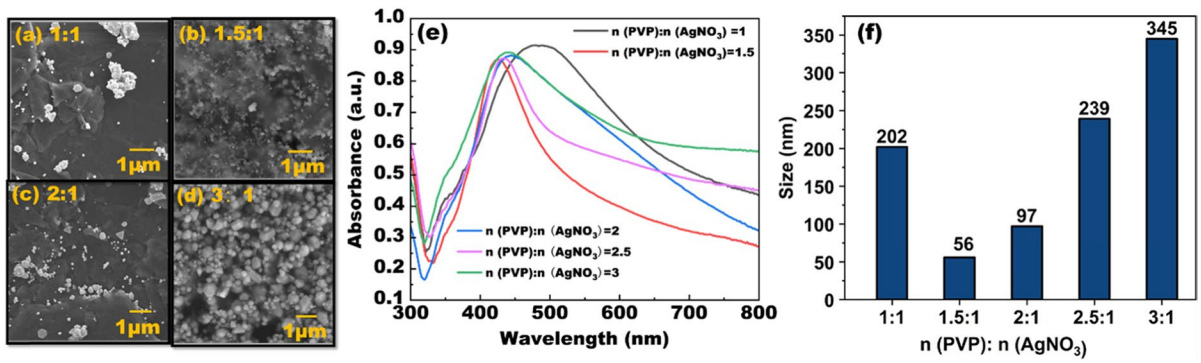

Fig. 4 SEM images of Ag NPs@graphene nanocomposite prepared by **a** PVP:$AgNO_3$ = 1:1, **b** PVP:$AgNO_3$ = 1.5:1, **c** PVP:$AgNO_3$ = 2:1, and **d** PVP:$AgNO_3$ = 3:1. **e** Corresponding to UV-vis absorption spectra. **f** Corresponding to statistics of Ag nanoparticle size

and sharp; and the intensity in the long wavelength region decreased, indicating that the size of Ag nanoparticles decreased; and the size distribution became narrow [39]. When the molar ratio of PVP to $AgNO_3$ increased from 1.5:1 to 3:1, it could be seen that the absorption peak moved to the long wavelength region and the absorbance in the long wavelength region showed a gradually increasing trend, indicating that the average size of the Ag nanoparticles was increasing, and the size distribution was becoming wider.

As shown in Fig. 4 f, with the increase of the PVP added before the reaction, the size of the Ag nanoparticles decreased first and then increased. When PVP interacted with Ag nanoparticles, PVP molecules would selectively adsorb on specific crystal planes, so the growth rate of this crystal plane was different from that of other crystal planes because of steric hindrance, thus controlling the morphology of Ag nanoparticles [40]. Appropriate amount of PVP could effectively prevent the agglomeration of Ag nanoparticles, enhance the stability of the particles, and obtain spherical Ag nanoparticles with narrow particle size distribution, good dispersion, and pure phase cubic crystal system [41–43]. When the concentration of PVP was low, the surface of the particles cannot be completely covered. Under the combined action of thermal motion and Brownian motion, the particles were prone to collision and agglomeration. At the same time, the polymer chain adsorbed on one surface would adhere to the surface of another uncovered particle and pull two or more particles together by bridging, causing flocculation. When PVP was excessive, supersaturated adsorption was achieved, and the surfactant would associate into micelles through the hydrophobic effect of the hydrocarbon chain, causing the particles to agglomerate and poor dispersion. At the same time, the viscosity of the solution increased, making it difficult to separate the particles, which brought trouble to the subsequent treatment. Therefore, the amount of PVP had an optimal value to ensure the preparation of Ag nanoparticles with smaller particle size and full dispersion. According to the experimental results, when the molar ratio of PVP to $AgNO_3$ was 1.5:1, the average size of Ag nanoparticles was the smallest (56 nm), the particle size distribution was uniform that can be seen from the SEM image and UV-vis absorption spectra. Therefore, the molar ratio of PVP to $AgNO_3$ of 1.5:1 was selected as the best reaction condition.

Mass ratio of graphite to $AgNO_3$

According to the previous research on graphene stripping by the research group, the optimal conditions for the mechanical stripping process of graphene had been determined [44]. Therefore, to explore the influence of the mass ratio of graphite to $AgNO_3$ on the properties of the Ag NPs@graphene nanocomposite, the amount of graphite was set to 0.5 g, and the mass ratios of graphite to $AgNO_3$ in this experiment were set to 2:1, 1:1,1:2, 1:3, and 1:4, respectively. The other conditions were fixed as the molar ratio of PVP to $AgNO_3$ was 1.5:1; the concentration of glucose solution was 0.3 mol/L; and the reaction temperature was 60 °C.

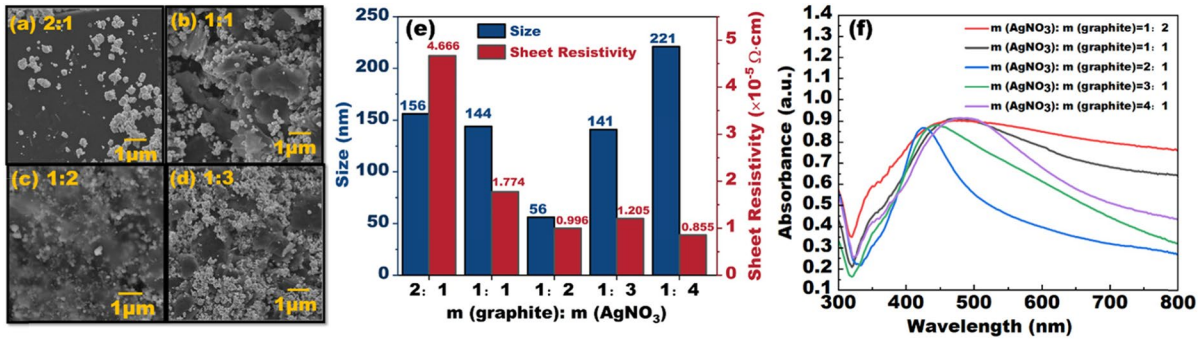

Fig. 5 SEM images of Ag NPs@graphene nanocomposite prepared by **a** m(graphite):m($AgNO_3$) = 2:1, **b** m(graphite):m($AgNO_3$) = 1:1, **c** m(graphite):m($AgNO_3$) = 1:2, and **d** m(graphite):m($AgNO_3$) = 1:3. e Corresponding to statistics of Ag nanoparticle size and Ag NPs@graphene nanocomposite resistivity. **f** Corresponding to UV-vis absorption spectra.

It can be seen from the SEM images (Fig. 5a–d) that when the mass ratio of graphite to $AgNO_3$ was 2:1 (Fig. 5a), the large Ag nanoparticle size (156 nm) and resistivity (4.666×10^{-5} Ω·cm) were found in Fig. 5 e. With the increase of the amount of $AgNO_3$, the average size of Ag nanoparticles began to decrease. When the mass ratio of graphite to $AgNO_3$ was 1:2, the size of Ag nanoparticles loaded on the prepared graphene was the smallest (56 nm, Fig. 5e) and distributed. The same conclusion could be drawn from UV-vis absorption spectra of Ag NPs@graphene nanocomposite (Fig. 5f). The symmetrical and sharp absorption peak appeared at the smallest position (426 nm). Moreover, the resistivity of the Ag NPs@graphene nanocomposite was relatively smaller (9.96×10^{-6} Ω·cm, Fig. 5e), which indicated that a large number of Ag nanoparticles and graphene formed a more complete conductive network. When the amount of $AgNO_3$ continued to increase, the average size of Ag nanoparticles began to increase (from 56 to 221 nm), and the dispersion of the composites became worse.

According to Weimarn's rule [45], the particle size of the precipitated particles depended on the nucleation rate and growth rate of the crystal nucleus, both of which were related to the concentration of the reactants. When the concentration of Ag^+ was low, and the supersaturation was slightly greater than the minimum supersaturation concentration of its nucleation (m(graphite):m($AgNO_3$) = 2:1–1:1), the growth rate of the nucleus was greater than the nucleation rate, and the silver atoms consumed by the growth per unit time were more than consumed by the nucleation of the nucleus. The nucleation of the nucleus was inhibited, resulting in a larger average particle size of Ag nanoparticles. Only when the growth rate and nucleation rate of the crystal nucleus were balanced, the Ag nanoparticles with smaller size and full dispersion could be obtained. With the increase of Ag^+ concentration (m(graphite):m($AgNO_3$) = 1:3–1:4), the growth rate of the crystal nucleus once again exceeded the nucleation rate, and a large number of crystal nuclei generated rapidly at the beginning of the reaction. Subsequently, most of the reduced silver atoms were consumed by the growth of the silver crystal nucleus, and the filling density of the crystal nucleus was very large, resulting in coagulation and growth between crystal nuclei [46], so the average particle size increased and the dispersion became worse.

Compared with mass ratio of graphite to $AgNO_3$ was 1:4, the condition of m(graphite):m($AgNO_3$) = 1:2 used less $AgNO_3$, but achieved almost similar resistivity, which was beneficial to reduce production costs. In addition, due to the size effect of Ag nanoparticles, silver nanoparticles with small particle size had a lower melting point [47–49], which was beneficial to reduce the sintering temperature of ink. Therefore, based on the above analysis, the mass ratio of $AgNO_3$ to graphite of 2:1 was selected as the best reaction condition.

Reductant concentration

To explore the effect of the concentration of reducing agent on the properties of the prepared Ag NPs@graphene nanocomposite, a set of comparative experiments of the concentration of reducing agent (glucose aqueous solution) of 0.3, 0.5, 1, 1.5, and 2 mol/L were designed. The other conditions were fixed as the molar ratio of PVP to $AgNO_3$ was 1.5:1; the mass ratio of $AgNO_3$ to graphite was 2:1; and the reaction temperature was 60 °C.

From the characterization results of SEM (Fig. 6a–d) and the statistical results of the average size of Ag nanoparticles (Fig. 6e), it could be seen that with the increase of the concentration of the glucose, the average size of the Ag nanoparticles and the resistivity of the Ag NPs@graphene nanocomposite showed a gradually increasing trend. When the concentration of glucose aqueous solution was 0.3~1 mol/L, the average size of the Ag nanoparticles was relatively small (56~58 nm). When the concentration of glucose increased to 2 mol/L, the average size of Ag nanoparticles increased to 113 nm. Similarly, the characterization results of UV-vis absorption spectra (Fig. 6f) showed that with the increase of the concentration of glucose, the UV-vis absorption peak of Ag nanoparticles shifted to the long wavelength region, and the absorbance in the long wavelength region showed an increasing trend, indicating that the average size of Ag nanoparticles increased, and the size distribution became wider. When the concentration of glucose was 0.3 mol/L, the average size of Ag nanoparticles was the smallest (56 nm, in Fig. 6e) and the conductivity of the Ag NPs@graphene nanocomposite was the best (1.243×10^{-5} Ω·cm, in Fig. 6e).

Controlling the concentration of the reducing agent was actually to control the reduction rate. When the concentration of the reducing agent was large, the reducing agent would reduce a large number of Ag nanoparticles nuclei in a short time, so PVP could not adsorb on the surface of Ag nanoparticles

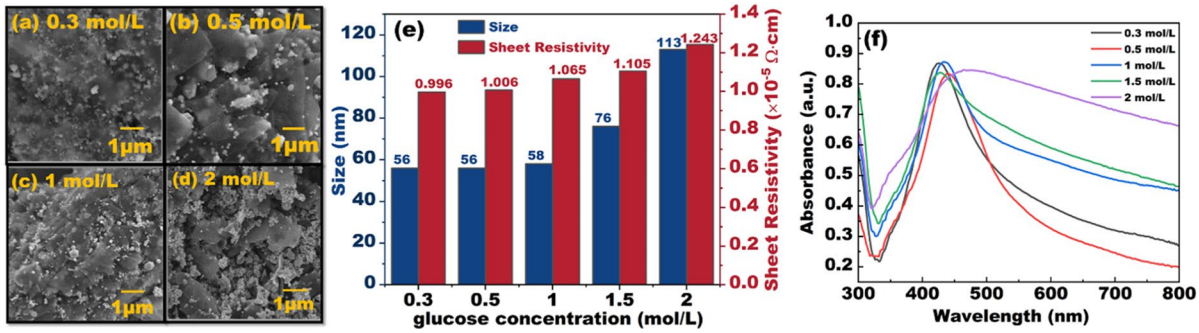

Fig. 6 SEM images of Ag NPs@graphene nanocomposite prepared by the glucose concentration of **a** 0.3 **b** 0.5 **c** 1, and **d** 2 mol/L. **e** Corresponding to statistics of Ag nanoparticle size and Ag NPs@graphene nanocomposite resistivity. **f** Corresponding to UV-vis absorption spectra

in time, causing the agglomeration of Ag nanoparticles and making the size of Ag nanoparticles larger [50]. Therefore, based on the above analysis of the prepared Ag NPs@graphene nanocomposite, the concentration of glucose of 0.3 mol/L was selected as the optimal reaction condition.

Reaction temperature

To explore the effect of reaction temperature on the properties of the prepared Ag NPs@graphene nanocomposite, a set of comparative experiments were designed with the reaction temperature of 30, 40, 50, 60, and 70 °C. The other conditions were fixed as the molar ratio of PVP to $AgNO_3$ was 1.5:1; the mass ratio of $AgNO_3$ to graphite was 2:1; and the concentration of the reducing agent was 0.3 mol/L.

It can be seen from the SEM images (Fig. 7a–d) and the average size statistics that when the reaction temperature was between 30 and 50 °C (Fig. 7a–b), the average size of Ag nanoparticles was larger (241~291 nm, Fig. 7e). When the reaction temperature rose to 60 °C (Fig. 7c), it could be clearly seen from the SEM image that Ag nanoparticles had dispersed sufficiently. The statistics data showed that the average size of Ag nanoparticles was the smallest (56 nm, Fig. 7e), and the resistivity was at the lowest level (9.45×10^{-6} Ω·cm, Fig. 7e). After increasing the reaction temperature to 70 °C (Fig. 7d), the average size of Ag nanoparticles began to increase again (150 nm), and the dispersion became worse. Similarly, the characterization results of UV-vis absorption spectra also confirmed above conclusions (Fig. 7f).

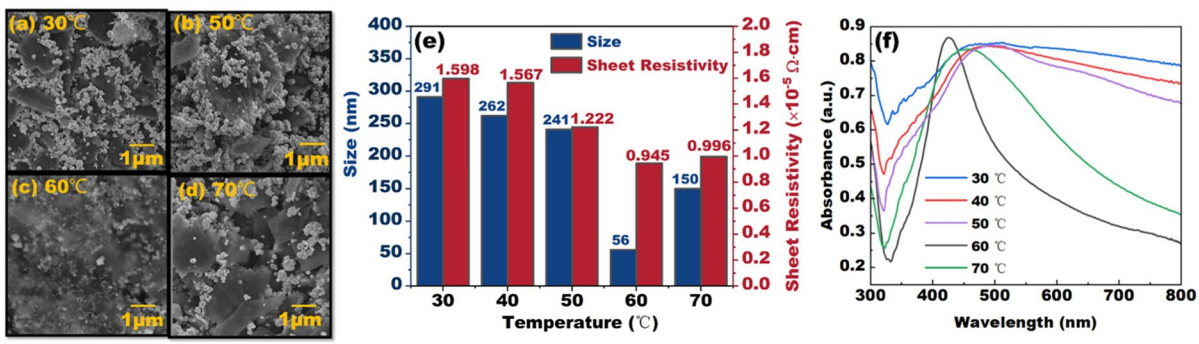

Fig. 7 SEM images of Ag NPs@graphene nanocomposite prepared by the reaction temperature **a** 30 °C, **b** 50 °C, **c** 60 °C, and **d** 70 °C. **e** Corresponding to statistics of Ag nanoparticles size and Ag NPs@graphene nanocomposite resistivity. **f** Corresponding to UV-vis absorption spectra

When the reaction temperature was low (30~50 °C), the reduction ability of glucose was weak. As a result, the initial nucleation particles would consume most of the reduced silver atoms, and the time of interaction between particles was prolonged, so the particle size of Ag nanoparticles was larger. When the temperature reached to 60 °C, the reduction of silver ions was faster. A large number of silver atoms were generated in a short time, and the nucleation rate was greatly improved. The nucleation process consumed most of the silver supply, which inhibited the growth of newly formed particles. Therefore, increasing the reaction temperature within a certain range was beneficial to the formation of silver nanoparticles with smaller particle size. This result was supported by Ref. [51, 52]. If the reaction temperature continued to rise (70 °C), the Brownian motion of the particles in the solution would increase, and the collision between the generated silver nanoparticles would continue to occur, resulting in the agglomeration of nanoparticles [53]. So the particle size began to increase again. Therefore, based on the above analysis of the prepared Ag NPs@graphene nanocomposite, the reaction temperature of 60 °C was selected as the best reaction condition.

Electrical properties of prepared inks

The conductive filler was dispersed in the binder to form a conductive ink, and the resin in the binder mainly played a bonding role between the conductive filler and the substrate material. To make the printed ink after sintering could have ideal electrical conductivity, it was necessary to make the printed ink track closely arranged together to form a path. Sintering was a necessary process to convert relatively independent Ag nanoparticles into continuous patterns [54, 55]. Sintering can be divided into high temperature sintering, chemical sintering, electrical sintering, plasma sintering, photonic sintering, and microwave sintering [56]. This paper used high temperature sintering treatment. The sintering time was also an important factor affecting the conductivity of the printed patterns. Appropriate sintering temperature and time could make Ag nanoparticles and graphene building tighter conductive networks [57].

After the printed patterns were sintered by a muffle furnace at suitable sintering temperature and time, the organic solvents and additives in the ink were volatilized successively, and the Ag nanoparticles and graphene were interconnected to form a conductive path. To explore the best sintering temperature and sintering time so that the printed patterns obtained the best electrical conductivity, two groups of experiments were designed to verify the relationship between sintering time and sintering temperature to the square resistance of the printed patterns.

Figure 8 a shows the square resistance of the printed patterns with sintering temperature of 80, 100, 150, 200, and 250 °C for 10 min. As the sintering temperature increased, the square resistance of the printed patterns decreased. It could be seen that the printed patterns were conductive at a low sintering temperature of 80 °C, but the square resistance was relatively high (2.1 Ω sq^{-1}). When the sintering temperature further increased, the square resistance of the printed patterns decreased significantly at 100 °C (64 mΩ sq^{-1}). It showed that the solvent and additive were effectively

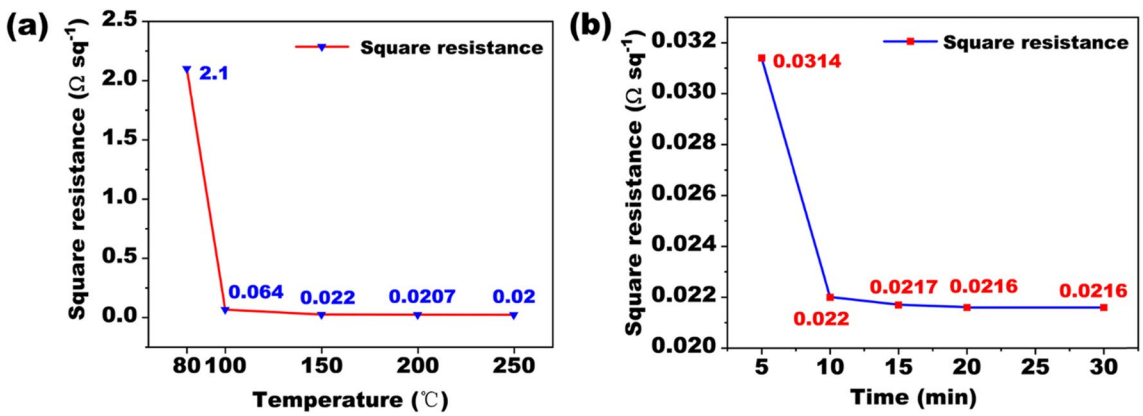

Fig. 8 **a** Effect of sintering temperature on square resistance. **b** Effect of sintering time on square resistance

Table 1 A comparative study of the present work with previously reported graphene/Ag ink papers

Conductive filler	Conductivity	Substrate	Sintering conditions	Ref.
rGO/Ag NWs	1.5 kΩ sq^{-1}	-	-	[65]
Ag/rGO	1.47×10^{-5} Ω·cm	PI	230 °C for 1 h	[66]
Ag nanotriangle platelet-rGO	170 Ω sq^{-1}	Glass wafers	Reduced in hydrazine vapor at 110 °C	[67]
Graphene-silver	0.08–4.74 Ω sq^{-1}	PEL paper	150 °C for 1 h	[68]
Graphene/Ag	5×10^{-6} Ω·m	Art paper	150 °C for 3 h	[58]
Graphene-silver	$< 10^{-6}$ Ω·m	PET/photo paper	100 °C for 20 min	[59]
Graphene/Ag	20 ± 1 Ω sq^{-1}	PI	400 °C for 30 min	[69]
Graphene/Ag	6.6×10^{-7} Ω•m	PI	150 °C for 20 min	This work

evaporated at this time. As the sintering temperature continued to increase, the square resistance of the printed patterns further reduced, which reached a minimum of 20 mΩ sq^{-1} at 250 °C, indicating that the increase of the sintering temperature could effectively remove the non-conductive components and successfully melted the Ag nanoparticles to form a conductive path with graphene [58–63]. However, considering the temperature that the substrates could withstand and the square resistance of the printed patterns had reached a relatively low level (22 mΩ sq^{-1}) at 150 °C. Therefore, 150 °C was selected as the best sintering temperature.

To further study the effect of sintering time on the square resistance of the printed patterns, the printed patterns were sintered at 150 °C for 5 min, 10 min, 15 min, 20 min, and 30 min, respectively. As shown in °. 8 b, the square resistance of the printed patterns decreased significantly at first and then kept stable with the increase of the sintering time. When the sintering time was 10 min, the square resistance of the printed patterns decreased to 22 mΩ sq^{-1}. This was because as the sintering time increased, the Ag nanoparticles melted further and grow sintering necks [64]. The sintering necks were connected with the graphene, which made the conductive network denser, improving the conductivity of the printed patterns. After extending the sintering time to 20 min, the square resistance of the printed patterns was reduced to the minimum (21.6 mΩ sq^{-1}). Therefore, 20 min was selected as the best sintering time. The average coating thickness of the printed patterns (sintered at 150 °C for 20 min) measured by a micrometer was 0.06 mm. Then the resistivity ρ of the coating could be calculated according to Formula (1).

$$R_s = \frac{\rho}{w} \quad (1)$$

where R_s is square resistance, Ω; w is the thickness, m.

The resistivity of the printed patterns was calculated to be 6.6×10^{-7} Ω•m. A comparative study of previously reported graphene/Ag ink based literature is listed in Table 1.

Conclusion

In the present study, a facile and effective in situ growth of Ag nanoparticles on pristine graphene to prepare Ag NPs@graphene nanocomposite was successfully proposed. The low-speed mechanical agitation and low-power sonication were combined to exfoliate the graphite, then glucose was used to reduce Ag^+ to obtain Ag nanoparticles in situ loaded on graphene. In the process of preparation of Ag NPs@graphene nanocomposite, the effects of the molar ratio of PVP to $AgNO_3$, the mass ratio of $AgNO_3$ to graphite, the concentration of glucose, and the reaction temperature on the properties of the Ag NPs@graphene nanocomposite were investigated. Finally, the optimum conditions for the preparation of Ag NPs@graphene nanocomposite were determined, as the molar ratio of PVP to $AgNO_3$ was 1.5:1; the mass ratio of $AgNO_3$ to graphite was 2:1; the concentration of reducing agent was 0.3 mol/L; and the reaction temperature was 60 °C. At the optimal conditions, the average size of the Ag nanoparticles was 56 nm, the Ag nanoparticles were uniformly attached to the graphene, and the two components make a good combination with each other. When sintered at 150 °C for 20 min, the square resistance of the patterns printed on the flexible PI substrates was 21.6 mΩ sq^{-1}, and the patterns were firmly attached

to the substrates. The results proved that the prepared Ag NPs@graphene nanocomposite water-based conductive ink had broad application prospects in printing flexible electronic products.

Data and code availability Not applicable

Author contributions Lei Zhu led all the experimental work and wrote the paper. Qin-Qin Xu and Jian-Zhong Yin supervised the project. Jin Guo, Shuo-Lei Niu, and Bao-Ning Lu participated in the experiments. All the authors participated in the discussion and preparation of the manuscript.

Funding The National Natural Science Foundation of China (21978043) and the National Key R&D Program of China (2020YFA0710202) support this research. The authors of this paper appreciate the funding organization.

Compliance with ethical standards

Ethical approval Not applicable

Conflict of interest The authors declare no competing interests.

References

1. Byeong-Ung H, Arsalan Z, Quang TT, Long W, Deuk LJ, Choi Y et al (2019) A transparent stretchable sensor for distinguishable detection of touch and pressure by capacitive and piezoresistive signal transduction. Npg Asia Mater 11(1). https://doi.org/10.1038/s41427-019-0126-x
2. Silva ZJ, Valenta CR, Durgin GD (2021) Optically transparent antennas: a survey of transparent microwave conductor performance and applications. Ieee Antennas Propag Mag 63(1):27–39. https://doi.org/10.1109/MAP.2020.2988526
3. Jung E, Kim C, Kim M, Chae H, Cho JH, Cho SM (2017) Roll-to-roll preparation of silver-nanowire transparent electrode and its application to large-area organic light-emitting diodes. Org Electron 41:190–197. https://doi.org/10.1016/j.orgel.2016.11.003
4. Yao S, Cui J, Cui Z, Zhu Y (2017) Soft electrothermal actuators using silver nanowire heaters. Nanoscale 9(11):3797–3805. https://doi.org/10.1039/C6NR09270E
5. Aburas M, Soebarto V, Williamson T, Liang R, Ebendorff-Heidepriem H, Wu Y (2019) Thermochromic smart window technologies for building application: a review. Appl Energy 255:113522. https://doi.org/10.1016/j.apenergy.2019.113522
6. Liu C, Balin I, Magdassi S, Abdulhalim I, Long Y (2015) Vanadium dioxide nanogrid films for high transparency smart architectural window applications. Opt Express 23(3):A124. https://doi.org/10.1364/OE.23.00A124
7. Jeon I, Yoon J, Kim U, Lee C, Xiang R, Shawky A et al (2019) High-performance solution-processed double-walled carbon nanotube transparent electrode for perovskite solar cells. Adv Energy Mater 9(27):1901204. https://doi.org/10.1002/aenm.201901204
8. Zhao P, Tang Q, Zhao X, Tong Y, Liu Y (2018) Highly stable and flexible transparent conductive polymer electrode patterns for large-scale organic transistors. J Colloid Interface Sci 520:58–63. https://doi.org/10.1016/j.jcis.2018.02.063
9. Ning J, Hao L, Jin M, Qiu X, Shen Y, Liang J et al (2017) A facile reduction method for roll-to-roll production of high performance graphene-based transparent conductive films. Adv Mater 29(9). https://doi.org/10.1002/adma.201605028
10. Teymouri A, Pillai S, Ouyang Z, Hao X, Liu F, Yan C et al (2017) Low-temperature solution processed random silver nanowire as a promising replacement for indium tin oxide. Acs Appl Mater Interfaces 9(39):34093–34100. https://doi.org/10.1021/acsami.7b13085
11. Li B, Ye S, Stewart IE, Alvarez S, Wiley BJ (2015) Synthesis and purification of silver nanowires to make conducting films with a transmittance of 99%. Nano Lett 15(10):6722–6726. https://doi.org/10.1021/acs.nanolett.5b02582
12. Rizwan M, Kutty AA, Kgwadi M, Drysdale TD, Sydanheimo L, Ukkonen L et al (2017) Possibilities of fabricating copper-based RFID tags with photonic-sintered inkjet printing and thermal transfer printing. Ieee Antennas Wirel Propag Lett 16:1828–1831. https://doi.org/10.1109/LAWP.2017.2682319
13. Das Neves MFF, Damasceno JPV, Junior ODL, Zarbin AJG, Roman LS (2021) Conductive ink based on PEDOT nanoparticles dispersed in water without organic solvents, passivant agents or metallic residues. Synth Met 272:116657. https://doi.org/10.1016/j.synthmet.2020.116657
14. Xu LY, Yang GY, Jing HY, Wei J, Han YD (2014) Ag-graphene hybrid conductive ink for writing electronics. Nanotechnology 25(5):55201. https://doi.org/10.1088/0957-4484/25/5/055201
15. Wu X, Niu F, Zhong A, Han F, Chen Y, Li J et al (2019) Highly sensitive strain sensors based on hollow packaged silver nanoparticle-decorated three-dimensional graphene foams for wearable electronics. Rsc Adv 9(68):39958–39964. https://doi.org/10.1039/C9RA08118F
16. He Y, Wu D, Zhou M, Zheng Y, Wang T, Lu C et al (2021) Wearable strain sensors based on a porous polydimethylsiloxane hybrid with carbon nanotubes and graphene. Acs Appl Mater Interfaces 13(13):15572–15583. https://doi.org/10.1021/acsami.0c22823
17. Maurya D, Khaleghian S, Sriramdas R, Kumar P, Kishore RA, Kang MG et al (2020) 3D printed graphene-based self-powered strain sensors for smart tires in autonomous vehicles. Nat Commun 11(1):5392. https://doi.org/10.1038/s41467-020-19088-y
18. Zhang X, Yan X, Chen J, Zhao J (2014) Large-size graphene microsheets as a protective layer for transparent conductive silver nanowire film heaters. Carbon N Y 69:437–443. https://doi.org/10.1016/j.carbon.2013.12.046
19. Xu C, Wang X (2009) Fabrication of flexible metal-nanoparticle films using graphene oxide sheets as substrates.

Small 5(19):2212–2217. https://doi.org/10.1002/smll.200900548
20. Shen J, Shi M, Li N, Yan B, Ma H, Hu Y et al (2010) Facile synthesis and application of Ag-chemically converted graphene nanocomposite. Nano Res 3(5):339–349. https://doi.org/10.1007/s12274-010-1037-x
21. Pasricha R, Gupta S, Srivastava AK (2009) A facile and novel synthesis of ag–graphene-based nanocomposites. Small 5(20):2253–2259. https://doi.org/10.1002/smll.200900726
22. Ren W, Fang Y, Wang E (2011) A binary functional substrate for enrichment and ultrasensitive SERS spectroscopic detection of folic acid using graphene oxide/ag nanoparticle hybrids. Acs Nano 5(8):6425–6433. https://doi.org/10.1021/nn201606r
23. Jasuja K, Berry V (2009) Implantation and growth of dendritic gold nanostructures on graphene derivatives: electrical property tailoring and Raman enhancement. Acs Nano 3(8):2358–2366. https://doi.org/10.1021/nn900504v
24. Mastalir Á, Király Z, Patzkó Á, Dékány I, Argentiere L (2008) Synthesis and catalytic application of Pd nanoparticles in graphite oxide. Carbon N Y 46(13):1631–1637. https://doi.org/10.1016/j.carbon.2008.06.054
25. Scheuermann GM, Rumi L, Steurer P, Bannwarth W, Muelhaupt R (2009) ChemInform Abstract: palladium nanoparticles on graphite oxide and its functionalized graphene derivatives as highly active catalysts for the Suzuki-Miyaura coupling reaction. ChemInform 40(45). https://doi.org/10.1002/chin.200945090
26. Yoo E, Okata T, Akita T, Kohyama M, Nakamura J, Honma I (2009) Enhanced electrocatalytic activity of Pt subnanoclusters on graphene nanosheet surface. Nano Lett 9(6):2255–2259. https://doi.org/10.1021/nl900397t
27. Zhou K, Zhao Y, Sun X, Yuan Z, Zheng G, Dai K et al (2020) Ultra-stretchable triboelectric nanogenerator as high-sensitive and self-powered electronic skins for energy harvesting and tactile sensing. Nano Energy 70:104546. https://doi.org/10.1016/j.nanoen.2020.104546
28. Chen S, Wei Y, Wei S, Lin Y, Liu L (2016) Ultrasensitive cracking-assisted strain sensors based on silver nanowires/graphene hybrid particles. Acs Appl Mater Interfaces 8(38):25563–25570. https://doi.org/10.1021/acsami.6b09188
29. Yang W, Wang C, Arrighi V, Vilela F (2017) One step synthesis of a hybrid Ag/rGO conductive ink using a complexation–covalent bonding based approach. Mater Sci Mater Electron 28(11):8218–8230. https://doi.org/10.1007/s10854-017-6533-2
30. Hareesh K, Williams JF, Dhole NA, Kodam KM, Bhoraskar VN, Dhole SD (2016) Bio-green synthesis of Ag–GO, Au–GO and Ag–Au–GO nanocomposites usingAzadirachta indica: its application in SERS and cell viability. Mater Res Express 3(7):75010. https://doi.org/10.1088/2053-1591/3/7/075010
31. Tien H, Huang Y, Yang S, Wang J, Ma CM (2011) The production of graphene nanosheets decorated with silver nanoparticles for use in transparent, conductive films. Carbon N Y 49(5):1550–1560. https://doi.org/10.1016/j.carbon.2010.12.022
32. Ferrari AC, Robertson J (2000) Interpretation of Raman spectra of disordered and amorphous carbon. Phys Rev B 61(20):14095–14107. https://doi.org/10.1103/PhysRevB.61.14095
33. Eckmann A, Felten A, Mishchenko A, Britnell L, Krupke R, Novoselov KS et al (2012) Probing the nature of defects in graphene by Raman spectroscopy. Nano Lett 12(8):3925–3930. https://doi.org/10.1021/nl300901a
34. Yu SJ, Yin YG, Chao JB, Shen MH, Liu JF (2014) Highly dynamic PVP-coated silver nanoparticles in aquatic environments: chemical and morphology change induced by oxidation of Ag(0) and reduction of Ag(+). Environ Sci Technol 48(1):403–411. https://doi.org/10.1021/es404334a
35. Tian L, Wang P, Zhao Z, Ji J (2013) Antimicrobial activity of electrospun poly(butylenes succinate) fiber mats containing PVP-capped silver nanoparticles. Appl Biochem Biotechnol 171(7):1890–1899. https://doi.org/10.1007/s12010-013-0461-2
36. Montazer M, Shamei A, Alimohammadi F (2012) Synthesizing and stabilizing silver nanoparticles on polyamide fabric using silver-ammonia/PVP/UVC. Prog Org Coat 75(4):379–385. https://doi.org/10.1016/j.porgcoat.2012.07.011
37. Ahlberg S, Antonopulos A, Diendorf J, Dringen R, Epple M, Flock R et al (2014) PVP-coated, negatively charged silver nanoparticles: a multi-center study of their physicochemical characteristics, cell culture and in vivo experiments. Beilstein J Nanotechnol 5:1944–1965. https://doi.org/10.3762/bjnano.5.205
38. Zhang Z, Zhang X, Xin Z, Deng M, Wen Y, Song Y (2011) Synthesis of monodisperse silver nanoparticles for ink-jet printed flexible electronics. Nanotechnology 22(42):425601. https://doi.org/10.1088/0957-4484/22/42/425601
39. Desai R, Mankad V, Gupta S, Jha P (2012) Size distribution of silver nanoparticles: UV-visible spectroscopic assessment. Nanosci Nanotechnol Lett 4(1):30–34. https://doi.org/10.1166/nnl.2012.1278
40. Chen Z, Chang JW, Balasanthiran C, Milner ST, Rioux RM (2019) Anisotropic growth of silver nanoparticles is kinetically controlled by polyvinylpyrrolidone binding. J Am Chem Soc 141(10):4328–4337. https://doi.org/10.1021/jacs.8b11295
41. Ruditskiy A, Xia Y (2016) Toward the synthesis of sub-15 nm Ag nanocubes with sharp corners and edges: the roles of heterogeneous nucleation and surface capping. J Am Chem Soc 138(9):3161–3167. https://doi.org/10.1021/jacs.5b13163
42. Yang TH, Zhou S, Gilroy KD, Figueroa-Cosme L, Lee YH, Wu JM et al (2017) Autocatalytic surface reduction and its role in controlling seed-mediated growth of colloidal metal nanocrystals. Proc Natl Acad Sci U S a 114(52):13619–13624. https://doi.org/10.1073/pnas.1713907114
43. Xia X, Zeng J, Oetjen LK, Li Q, Xia Y (2012) Quantitative analysis of the role played by poly(vinylpyrrolidone) in seed-mediated growth of Ag nanocrystals. J Am Chem Soc 134(3):1793–1801. https://doi.org/10.1021/ja210047e
44. Xu Q, Zhao W, Zhi J, Yin J (2018) Exfoliation of graphite in CO2 expanded organic solvents combined with low speed shear mixing. Carbon N Y 135:180–186. https://doi.org/10.1016/j.carbon.2018.03.040

45. Sugimoto T (2001) Monodispersed particles. Elsevier, pp 86–117
46. Vilvamani N, Gupta T, Gupta RD, Awasthi SK (2014) Bottom-up molecular-assembly of Ru(ii)polypyridyl complex-based hybrid nanostructures decorated with silver nanoparticles: effect of Ag nitrate concentration. Rsc Adv 4(38):20024–20030. https://doi.org/10.1039/C4RA01347F
47. Hong J, Ding Y, Moon K, Wong CP (2013) Enhanced diffusion of silver atoms on the surface of nanoparticles at low temperatures. J Electron Packag 135(1). https://doi.org/10.1115/1.4023910
48. Qi WH, Wang MP (2002) Size effect on the cohesive energy of nanoparticle. J Mater Sci Lett 21(22):1743–1745. https://doi.org/10.1023/a:1020904317133
49. Jiang H, Moon K, Dong H, Hua F, Wong CP (2006) Size-dependent melting properties of tin nanoparticles. Chem Phys Lett 429(4-6):492-496. https://doi.org/10.1016/j.cplett.2006.08.027
50. Tang BL, Chen GX, Chen QF, Tai JL (2011) Research on preparation of nano-silver by orthogonal test. Mater Sci Forum 694:142–145. https://doi.org/10.4028/www.scientific.net/MSF.694.142
51. Liguo Y, Yanhua Z (2010) Preparation of nano-silver flake by chemical reduction method. Rare Metal Mat Eng 39(3):401–404. https://doi.org/10.1016/S1875-5372(10)60088-4
52. Lee G (2004) Preparation of silver nanorods through the control of temperature and pH of reaction medium. Mater Chem Phys 84(2-3):197–204. https://doi.org/10.1016/j.matchemphys.2003.11.024
53. Yonghui S, Gongying L, Qiuli Z, Xuegang L, Chunyang W (2007) Research on preparation of spherical nanosized silvery powder. Rare Metal Mat Eng 36(4):709–712. https://doi.org/10.3321/j.issn:1002-185X.2007.04.033
54. Kang JS, Ryu J, Kim HS, Hahn HT (2011) Sintering of inkjet-printed silver nanoparticles at room temperature using intense pulsed light. J Electron Mater 40(11):2268–2277. https://doi.org/10.1007/s11664-011-1711-0
55. Dharmadasa R, Jha M, Amos DA, Druffel T (2013) Room temperature synthesis of a copper ink for the intense pulsed light sintering of conductive copper films. Acs Appl Mater Interfaces 5(24):13227–13234. https://doi.org/10.1021/am404226e
56. Wünscher S, Abbel R, Perelaer J, Schubert US (2014) Progress of alternative sintering approaches of inkjet-printed metal inks and their application for manufacturing of flexible electronic devices. J Mater Chem C Mater 2(48):10232–10261. https://doi.org/10.1039/C4TC01820F
57. Vo DQ, Shin EW, Kim JS, Kim S (2010) Low-temperature preparation of highly conductive thin films from acrylic acid-stabilized silver nanoparticles prepared through ligand exchange. Langmuir 26(22):17435–17443. https://doi.org/10.1021/la102627m
58. Li W, Yan J, Wang C, Zhang N, Choy TH, Liu S et al (2022) Molecule bridged graphene/Ag for highly conductive ink. Sci China Mater 65(10):2771–2778. https://doi.org/10.1007/s40843-022-2064-8
59. Zhao J, Song M, Wen C, Majee S, Yang D, Wu B et al (2018) Microstructure-tunable highly conductive graphene-metal composites achieved by inkjet printing and low temperature annealing. J Micromech Microeng 28(3):35006. https://doi.org/10.1088/1361-6439/aaa450
60. Wang F, Zhu H, He H (2016) Low temperature sintering of Ag nanoparticles/graphene composites for paper based writing electronics. J Phys D Appl Phys 49(41):415501. https://doi.org/10.1088/0022-3727/49/41/415501
61. Liu P, He W, Lu A (2019) Preparation of low-temperature sintered high conductivity inks based on nanosilver self-assembled on surface of graphene. J Cent South Univ 26(11):2953–2960. https://doi.org/10.1007/s11771-019-4227-z
62. Liu P, Ma J, Deng S, Zeng K, Deng D, Xie W et al (2016) Graphene-Ag nanohexagonal platelets-based ink with high electrical properties at low sintering temperatures. Nanotechnology 27(38):385603. https://doi.org/10.1088/0957-4484/27/38/385603
63. Zou Q, Cao C, Zhu H, Hou C (2019) In: Zhao P, Ouyang Y, Xu M, Yang L, Ren Y (eds) (2019-1-1). Preparation of low temperature sintered graphene/silver nanocomposite-based conductive ink. Springer Singapore, pp 751–758
64. Jiang H, Liang S, Wei C, Ke C (2022) Phase field modelling of the electromigration behaviour in sintered silver. J Mater Res 37(14):2322–2334. https://doi.org/10.1557/s43578-022-00635-w
65. Giasafaki D, Mitzithra C, Belessi V, Filippakopoulou T, Koutsioukis A, Georgakilas V et al (2022) Graphene-based composites with silver nanowires for electronic applications. Nanomaterials (Basel) 12(19). https://doi.org/10.3390/nano12193443
66. Yang W, Wang C, Arrighi V, Vilela F (2017) One step synthesis of a hybrid Ag/rGO conductive ink using a complexation–covalent bonding based approach. J Mater Sci Mater Electron 28(11):8218–8230. https://doi.org/10.1007/s10854-017-6533-2
67. Li L, Guo Y, Zhang X, Song Y (2014) Inkjet-printed highly conductive transparent patterns with water based Ag-doped graphene. J Mater Chem. A, Mater Energy Sustain 2(44):19095–19101. https://doi.org/10.1039/C4TA04156A
68. Karim N, Afroj S, Tan S, Novoselov KS, Yeates SG (2019) All inkjet-printed graphene-silver composite ink on textiles for highly conductive wearable electronics applications. Sci Rep 9(1):8035. https://doi.org/10.1038/s41598-019-44420-y
69. Deng D, Feng S, Shi M, Huang C (2017) In situ preparation of silver nanoparticles decorated graphene conductive ink for inkjet printing. J Mater Sci Mater Electron 28(20):15411–15417. https://doi.org/10.1007/s10854-017-7427-z